This is the authors' version of a paper with reference: Decao Yin, Elizabeth Passano, Halvor Lie, Guttorm Grytøyr, Kristoffer Aronsen, Michael Tognarelli, Elizbar Buba Kebadze (2019) Experimental and numerical study of a top tensioned riser subjected to vessel motion. in Ocean Engineering, Volume 171, 1 January 2019, Pages 565-574
The version of record is available at:
https://doi.org/10.1016/j.oceaneng.2018.12.029

Experimental and numerical study of a top tensioned drilling riser subjected to vessel motion

Decao Yin[a,*], Elizabeth Passano[a], Halvor Lie[a], Guttorm Grytøyr[b], Kristoffer Aronsen[b], Michael Tognarelli[c], Elizbar Buba Kebadze[d]

[a]*SINTEF Ocean, Trondheim, Norway*
[b]*Statoil, Oslo, Norway*
[c]*BP, Houston, Texas, USA*
[d]*BP Exploration Operating Company Ltd, Sunbury on Thames, UK*

Abstract

Model tests of a top tensioned riser (TTR) model were carried out as a part of a joint industry project, with the purpose of better understanding the dynamic behaviour of drilling riser and verifying the calculations of the riser analysis tools. Sinusoidal motion in one direction was imposed at the top end of the riser model to simulate vessel motion. The tests were carried out in still water, accelerations and bending strains were measured along the riser model. Numerical simulations were performed using RIFLEX and the predicted global responses were compared with the model tests. This paper discusses interesting aspects of this comparison as well as the general dynamic behaviour of the top tensioned riser.

It was found that the dynamic responses of a TTR with vessel motion can consist of not only the IL responses due to vessel motion at the riser top end, but also CF vortex-induced vibrations (VIV) under conditions when Keulegan–Carpenter (KC) number is relatively small. CF VIV response is estimated using a time domain VIV prediction model and compared to the measured response. The main conclusion is that the IL global dynamic responses and CF VIV responses are predicted sufficiently well.

Keywords: Vortex-induced vibrations, Top-tensioned riser, Keulegan–Carpenter number, Time domain

1. Introduction

A top tensioned marine riser connects the offshore wellhead (WH) on the seabed and the mobile offshore drilling unit (MODU) on the free surface, conveying oil and mud. The marine riser is subject to dynamic loads caused by waves, currents and motions of MODU induced by environmental loads (Yin et al., 2018a). The TTR system is developed for deepwater drilling and/or workover operations. TTR is widely deployed by spar or tensioned-leg platforms (TLP).

VIV of a free-hanging riser due to vessel motion have been investigated by both experimentally and numerically (Jung et al., 2012; Kwon et al., 2015; Wang et al., 2017b,c). Jung et al. (2012) carried out model tests on a scaled free-hanging riser with

*Corresponding author
Email address: decao.yin@sintef.no (Decao Yin)

imposed top oscillations in still water, and studied the VIV responses under low KC numbers (2 to 17). Kwon et al. (2015) studied an Ocean Thermal Energy Conversion (OTEC) riser by conducting IL forced oscillation experiments in designed current on a scaled OTEC riser model. The KC numbers are relatively low (2 to 4). It is found that due to the current, IL VIV responses were weakened, while CF VIV responses were amplified due to larger relative velocity. Wang et al. (2017b) performed model test on a free hanging riser with vessel motion in constant current, corresponding KC numbers are between 10 and 80. The out-of-plane VIV responses were observed and the resulted strain was comparable to the in-plane global responses. Wang et al. (2017c) proposed an empirical prediction methodology to account for vessel motion induced VIV for a free hanging riser under small KC numbers (8.3, 12.7).

Guo et al. (2013) investigated the dynamic responses of a TTR under combined excitation of vessel motion, surface wave and internal solitary wave. The riser is vibrating either at the surface wave frequency or vessel motion frequency, while the influence of internal solitary wave is much larger than the other two excitations.

Meng et al. (2017) modelled and simulated a flexible pipe conveying internal flow in its transition range from being subcritical to supercritical. A combination of internal flow effect and VIV was illustrated. Distinct different internal flow effect was identified depending on the velocity of the internal flow.

Wang et al. (2017a) investigated the VIV of a steel catenary riser (SCR) due to vessel motion, which is equivalent to oscillatory current. The dominant parameter - maximum equivalent current velocity is found to govern the vessel-motion induced VIV.

Shi and Manuel (2017) applied proper orthogonal decomposition (POD) and weighted waveform analysis (WWA)to the data sequentially to estimate the fatigue damage estimation in an instrumented riser effectively.

Thorsen et al. (2014) has developed a new semi-empirical time domain method for VIV prediction. It includes a hydrodynamic excitation force model in which the excitation force synchronizes with the oscillation velocity to obtain lock-in. Thorsen et al. (2016) extended the time domain method by adding a damping formulation, and the excitation force model was optimized by validation against flexible riser VIV tests. The optimized time domain model was used to simulate the CF VIV of an elastic cylinder in oscillating flow at two KC numbers (31 and 178) and maximum reduced velocities. Comparison with experiments shows that the model provides realistic frequency content, dominating mode and amplitude of vibration. Ulveseter et al. (2017) modified the time domain model by modelling the midpoint of the synchronization range as a simplified Gaussian process, and enable it to describe the stochastic stochastic nature of the responses of long slender beams subjected to stationary current.

Yuan et al. (2017) proposed another time domain model which can simulate combined CF and IL VIV. However, the hydrodynamic coefficient in IL direction was taken from pure IL experiments by Aronsen (Aronsen and Larsen, 2007; Aronsen, 2007), instead of combined IL and CF VIV experiments. The prediction is expected to be improved by using more realistic IL coefficients from combined IL and CF VIV experiments, such as Yin et al. (2018b).

Significant diverging conclusions on global riser analysis were found from different studies. For example, Tognarelli et al. (2008) concludes that '*For full scale drilling risers without VIV suppression, data show that state-of-the-art analysis methods are, on average, inherently 30X conservative on a maximum fatigue damage basis.*' While after comparing global riser analysis of a drilling riser with full scale measurement, Grytøyr et al. (2017) concluded that '*global riser analyses are able to predict the actual load levels with reasonable accuracy. However, the results actually indicate that there is a slight bias towards non-conservative results when studying the square root of sum of squares (SRSS) value of the response, especially for the lower riser response.*' The bias is mainly due to the scatter (spreading) in the measured signals, in addition, by adjusting the hydrodynamic coefficients in the prediction tools, the analysis could also be improved.

With review of the above research works, several conclusions could be made: (1) Risers under vessel motion will not only have the in-plane global responses, the out-of-plane VIV responses will also be excited; (2) The resultant strain in both directions are comparable and should be considered; (3) VIV due to vessel motion is equivalent to VIV in oscillatory flow, the dominant parameter is the KC number; (4) Time domain method is needed to predict the vessel motion induced VIV accurately.

Statoil and BP carried out a comprehensive model test program on drilling risers in MARINTEK's Towing Tank in February 2015 (Yin et al., 2018a). The objective was to validate and verify software predictions of drilling riser behaviour under various environmental conditions by using of model test data. The configurations of the model were varied systematically by including different lower boundary conditions, blow-out preventer (BOP) and lower marine riser package (LMRP), buoyancy modules and drill string. In the present paper we only study the top-tensioned bare riser model configuration under forced harmonic motion on the riser top end.

The present study focuses on the dynamic responses of a top-tensioned riser under vessel motions. Part of the results were published in Yin et al. (2018c).

2. Theoretical background

2.1. VIV in oscillatory flow

The problem studied in this paper is a top-tensioned riser model subjected to sinusoidal motion on the top end in still water, which is equivalent to a drilling riser subjected to oscillatory flow.

The IL hydrodynamic forces include an inertia force and a drag force, the CF hydrodynamic force is the fluctuating lift force due to vortex shedding (Blevins, 1990). When $KC > 30$, the vortex shedding period $T_s \approx 5D/\dot{x}_{max}$ is a small fraction of the oscillation period $T = KCD/\dot{x}_{max}$, where $\dot{x}_{max}$ is the maximum oscillating velocity, D is the outer diameter of the riser model. For our case $KC < 30$, the vortex shedding period is comparable to the oscillating period and strong interaction is expected.

After reviewing several earlier experimental work, (Blevins, 1990) classified the vortex shedding patterns of circular cylinders in oscillatory flow, and the relationship between vortex shedding frequency and oscillation frequency, see Tab. 1.

2.2. Parameters

Several key parameters are discussed and defined by Sumer and Fredsøe (1988) and Blevins (1990).

The forced harmonic motion at the top end of the riser $x(t)$ is:

$$\begin{aligned} x(t) &= Asin(\omega t) \\ &= Asin(\frac{2\pi}{T}t) = Asin(2\pi f t) \end{aligned} \tag{1}$$

where A is the oscillation amplitude, $\omega = 2\pi/T = 2\pi f$ is the angular oscillation frequency.

The oscillation velocity $\dot{x}(t)$ can be derived as:

$$\begin{aligned} \dot{x}(t) &= \omega Acos(\omega t) = \frac{2\pi}{T}Acos(\frac{2\pi}{T}t) \\ &= 2\pi f Acos(2\pi f t) \end{aligned} \tag{2}$$

Inserting the amplitude of the flow velocity, $2\pi A/T$, into the formula for the KC number gives:

$$KC = \frac{VT}{L} = \frac{2\pi A}{T}\frac{T}{D} = \frac{2\pi A}{D} \tag{3}$$

where V is the oscillating velocity, D is the outer diameter of the riser.

The Reynolds number is defined as

$$\begin{aligned} Re &= \frac{\dot{x}(t)D}{\nu} = \frac{2\pi AD}{\nu T}cos(\frac{2\pi}{T}t) \\ &= \frac{2\pi f AD}{\nu}cos(2\pi f t) \end{aligned} \tag{4}$$

The maximum Reynolds number can be found

$$Re_{max} = \frac{\dot{x}_{max}D}{\nu} = \frac{2\pi AD}{\nu T} = \frac{2\pi f AD}{\nu} \tag{5}$$

where ν is the kinematic viscosity of the fluid.

The reduced velocity V_r is defined as

$$V_r = \frac{\dot{x}_{max}}{Df_n} = \frac{2\pi Af}{Df_n} = \frac{2\pi A}{D}\frac{f}{f_n} \tag{6}$$

where f_n is the measured natural oscillation frequency in still water.

3. Model test

The model tests have been performed in the Towing Tank III at MARINTEK (now SINTEF Ocean), see Fig. 1. The Towing Tank III has a dimension of $L \times B \times D = 85\ m \times 10.5\ m \times 10\ m$. It is equipped with a double flap wave-maker and a overhead towing carriage. The model tests to be analysed in this paper is carried out in still water.

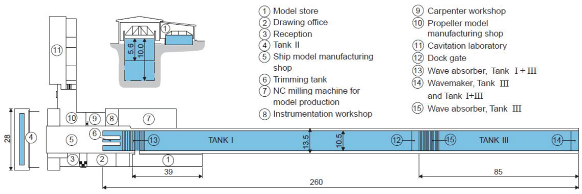

Figure 1: Principle sketch of the towing tank in SINTEF Ocean (earlier MARINTEK).

3.1. Test set-up

The general set-up of the model test is illustrated in Fig. 2. The test rig is a steel truss beam which accommodates the drilling riser model. The truss beam is hinged onto the vertical beams on the towing carriage, and it can be lifted to a horizontal position by the overhead crane on the towing carriage when rigging is needed. On the top side, steel substructures are added to enhance the stiffness of the rig and accommodate the horizontal oscillator. On the bottom side of the rig, four chains were spread

Table 1: Vortex shedding pattern and frequency ratio in oscillatory flow, from page 217 of (Blevins, 1990).

KC	Vortex pattern	f_{CF}/f
<0.4	No separation.	No CF forces
0.4 - 4	A symmetric pair of vortices is formed in the wake. The vortices reverse during the oscillation cycle	CF forces are minimal.
4 - 8	Asymmetric pair of vortices.	2
8 - 15	Vortex pairs are shed alternately into the wake during each half-cycle of oscillation. The vortex pairs convect alternately asymmetrically at $\approx 45\,\text{deg}$	2
15 - 22	Multiple pairs of vortices are shed per cycle and the pairs convect at 45 deg.	3
22 - 30	Multiple pairs of vortices are shed per cycle.	4
>30	Quasi-steady vortex shedding.	$\approx 0.2KC$

diagonally to keep the rig vertical and provide additional stiffness. The drilling riser model is pinned on both ends, and it is pre-tensioned by a compress spring on the top end. Harmonic motion is imposed on the top end by a linear motion system, see Fig. 3. The submerged part of the riser model is filled with fresh water.

3.2. Riser model

The core of the bare riser model was a fibreglass reinforced pipe. This core fibreglass pipe has an outer diameter of 20 mm and a wall thickness of 1.5 mm. It was fabricated by a subcontractor, Vello Nordic AS. The optical fibres, accelerometers, and their cables were glued on the outer surface of the fibreglass pipe. A silicon tube was wrapped around the sensors and cables. Due to the cables and silicon tube, the outer diameter of the riser model was increased to 28 mm generally.

At the locations of accelerometers, the outer diameter was slightly increased locally at the accelerometer locations. When the riser is vibrating, additional structural damping might be introduced by friction between silicon tube and the core fibreglass pipe. The local increase of outer diameter and possible structural damping due to friction were neglected in the numerical calculation.

The properties of the riser model in model scale (MS) and corresponding full scale (FS) values are summarized in Tab. 2. The drilling riser model is in 1:19 scale, and Froude scaling is applied in the present study.

3.3. Instrumentation and Data acquisition

The bare riser model was instrumented with fibre optics strain gauges at thirteen (13) locations along the riser. At each location, four fibre optics strain gauges were instrumented, implying 52 strain gages in total. They are used to measure axial stress and biaxial bending stresses. The fibres were glued on the glass fibre rod, in four quadrants of the cross section. The fibres were protected by

Table 2: Riser model properties.

Property	Unit	Model scale	Full scale
Outer diameter, OD	m	0.028	0.532
Inner diameter, ID	m	0.017	0.323
Length, L	m	8.996	171
Mass/length, m/l	kg/m	0.668	247
Bending stiffness, EI	Nm^2	120	3.5×10^8
Spring stiffness, K	N/m	1.819×10^5	6.73×10^7
Top tension, T	N	212	1.5×10^6

the outer silicon layer. Additionally, two normal strain gauges were instrumented. One is located on the bare riser top part, above the water line. One is located near the lower end of the riser. Twelve (12) two-dimensional accelerometers were instrumented on the bare riser. The fibre optic strain signals were sampled at a rate of 25 Hz. All other signals were sampled at a rate of 200 Hz. Figure 4 presents the distribution of accelerometers, fibre optic strain gauges, and strain gauges.

The displacement is obtained by integrating acceleration signals measured by accelerometers. The curvature are directly measured by both fibre optic strain gauges and normal strain gauges.

3.4. Test program

The complete test program and other configurations are described in Yin et al. (2018a).

The tests on the top-tensioned riser configuration are studied in this paper and listed in Tab. 3. Unidirectional sinusoidal oscillation motions were imposed on the top end of the riser model. Eigenvalue analysis was performed before the experiments, and pluck tests were carried out to verify the eigenfrequencies when the test model was set up. The oscillation frequency was either the 1^{st} eigenfrequency (Test 1015, Test 1020 and Test 1025) or the 2^{nd} eigenfrequency (Test 1005, Test 1010 and Test 1011), in order to excite the first or the second modes. Meanwhile, the two frequencies were considered to be representative for wave frequencies. Oscillation amplitudes were varied under each frequency.

4. Numerical simulation

The model test data is used to verify and validate numerical models. The top-tensioned riser model is numerically modelled using RIFLEX (SINTEF Ocean, 2017a). RIFLEX is an efficient program system for hydrodynamic and structural analysis of slender marine structures. It basically includes a finite element module which uses beam or bar elements, and a hydrodynamic loading model described by the generalised Morison's equation. In the present study, RIFLEX simulation is performed under SIMA (SINTEF Ocean, 2017b). SIMA is a workbench developed by SINTEF Ocean (former MARINTEK). It supports the entire process

Table 3: Test program.

Test No.	A [m] MS/FS	f [Hz] MS/FS	KC	Re_{max}
1005	0.026/0.50	1.477/0.399	5.83	5.93×10^3
1010	0.052/1.00	1.477/0.399	11.67	1.18×10^4
1011	0.013/0.25	1.477/0.399	2.92	2.96×10^3
1015	0.026/0.50	0.646/0.148	5.83	2.59×10^3
1020	0.052/1.00	0.646/0.148	11.67	5.19×10^3
1025	0.078/1.50	0.646/0.148	17.50	7.87×10^3

from the definition of the simulation and its execution to the interpretation and documentation of the results. The definition of a simulation is streamlined through a user-friendly graphical interface with three dimensional visualisation. It offers a complete solution for simulation and analysis of marine operations and floating systems.

4.1. Eigenvalue analysis

Eigenvalue analysis is performed to find the eigenfrequencies and corresponding eigenmodes.

4.2. IL responses modelling

The dynamic responses in IL direction is due to the imposed harmonic motion at the top end of the riser model.

Non-linear time domain global dynamic analysis is performed in IL direction (direction of oscillation) to simulate the dynamic responses in in-line direction. Morison's equation (Faltinsen, 1993; SINTEF Ocean, 2017a) is used to calculate the hydrodynamic force in IL direction.

4.3. CF responses modelling

To investigate and simulate the VIV in CF direction due to oscillatory flow, a recently developed time domain VIV prediction model is used Thorsen et al. (2014, 2016). This time domain VIV prediction model is implemented in RIFLEX now.

At any point along the riser, the total hydrodynamic force is calculated as:

$$\begin{aligned} \mathbf{F} &= C_M \rho \frac{\pi D^2}{4} \dot{\mathbf{u}}_n - (C_M - 1)\rho \frac{\pi D^2}{4} \ddot{\mathbf{x}}_n + \\ &= \frac{1}{2}\rho D C_D |\mathbf{v}_n| \mathbf{v}_n + \\ &= \frac{1}{2}\rho D C_v |\mathbf{v}_n| (\mathbf{j}_3 \times \mathbf{v}_n) cos\phi_{exc} \end{aligned} \tag{7}$$

The three first terms on the right side of Eq. (7) make up Morison's equation (Faltinsen, 1993), while the final term represents the oscillating lift force due to vortex shedding (SINTEF Ocean, 2017a). ρ is the water density, D is the outer diameter of the riser. C_M and C_D are the inertia and drag coefficients respectively, while C_v determines the strength of the vortex shedding force. Furthermore, $\dot{\mathbf{u}}_n$ is the normal component of the fluid particle acceleration which is perpendicular to the cylinder axis, $\ddot{\mathbf{x}}_n$ is the normal component of the cylinder

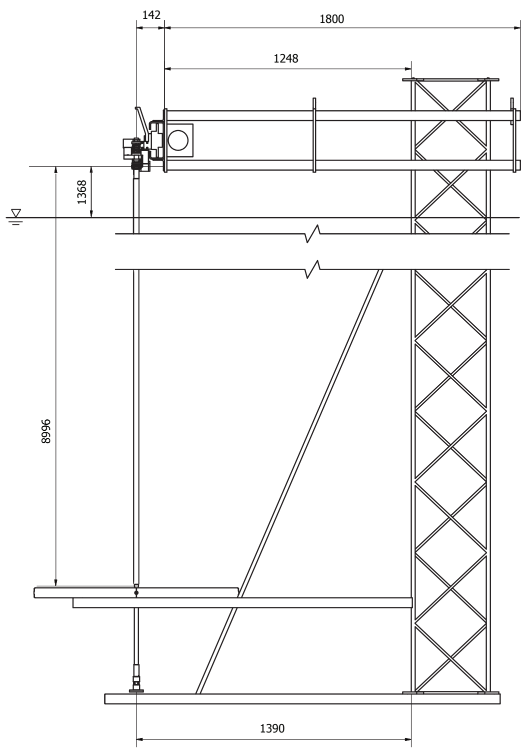

Figure 2: Model test set-up.

acceleration and $\ddot{\mathbf{v}}_n$ is the normal component of the relative fluid velocity. The relative flow velocity is given as $\mathbf{v} = \mathbf{u} - \dot{\mathbf{x}}$, where $\mathbf{u}$ is the incoming flow velocity and $\dot{\mathbf{x}}$ is the velocity of the cylinder cross-section. $\mathbf{j}_3$ is a unit vector pointing in the direction of the cylinder axis.

ϕ_{exc} is a time-varying phase that describes the oscillations of the lift force. The evolution in time is given by equations (8) and (9):

$$\frac{d\phi_{exc}}{dt} = 2\pi \frac{\hat{f}_{exc}|\mathbf{v}_n|}{D} \tag{8}$$

$$\hat{f}_{exc} = \begin{cases} \hat{f}_0 + (\hat{f}_{max} - \hat{f}_0) sin\theta, \ \theta \geq 0 \\ \hat{f}_0 + (\hat{f}_0 - \hat{f}_{min}) sin\theta, \ \theta < 0 \end{cases} \tag{9}$$

Equation (8) gives the relationship between the dimensionless and the actual frequency. Equation (9) models the synchronization between the vortex shedding and the cylinder motion. Here, θ is the instantaneous phase difference between the cylinder cross-flow velocity and the lift force. The essential feature of the synchronization model is that it is possible for the lift force to vary its instantaneous frequency between $\hat{f}_{min}$ and $\hat{f}_{max}$, and *lock on* to the frequency of vibration. For more details see Thorsen et al. (2014, 2016).

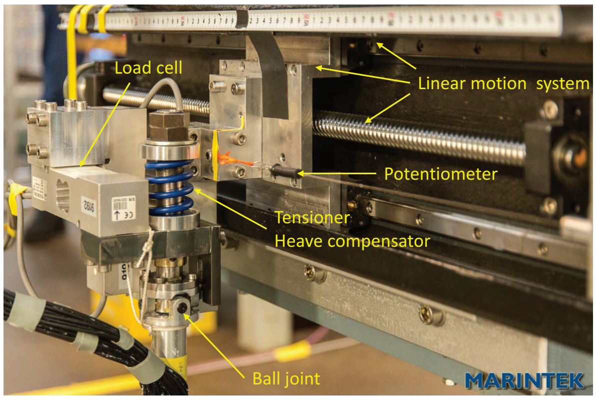

Figure 3: Riser top unit: One degree-of-freedom (DOF) forced motion actuator, tensioner/heave compensator, ball joint, horizontal potentiometer, and three component load cell.

The empirical parameters used in the present study are given in Tab. 4.

5. Results and discussions

5.1. *Eigenfrequencies and eigenmodes*

The first three normalized eigenvector shapes found from eigenvalue analysis in RIFLEX are shown in Fig. 5. Corresponding calculated eigenfrequencies are compared with measured eigenfrequencies from decay test in still water, see Tab. 5. The difference between calculated and measured eigenfrequencies are within 5%, which is acceptable. This difference might be due to the non-continuity

Table 4: Empirical parameters used in the hydrodynamic model.

C_M	C_D	C_v	$\hat{f}_0$	$\hat{f}_{min}$	$\hat{f}_{min}$
1.1	1.0	1.3	0.17	0.125	0.3

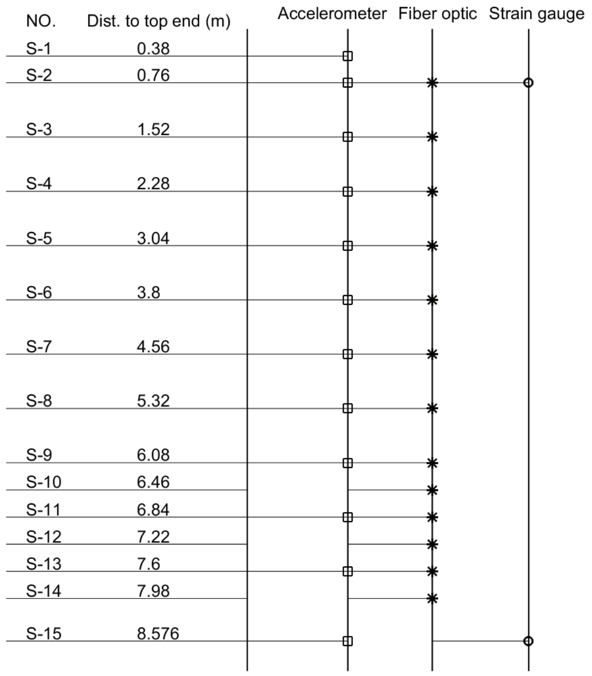

Figure 4: Instrumentation distribution.

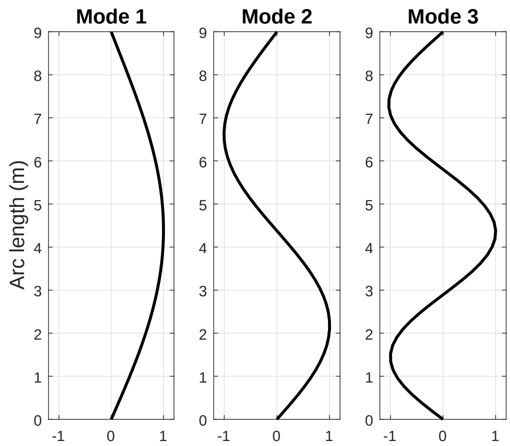

Figure 5: Eigenmodeshapes of displacement.

of the cross section along the riser, caused by the instrumentations.

5.2. Displacement amplitude and orbits

Figure 6 to Fig. 11 show the displacement responses of all tests listed in Tab. 3. In each figure, the plot on the left presents the normalized displacement amplitude along the riser model in both IL and CF directions. The plots on the two right columns show the orbits of twelve (12) cross sections with accelerometers (see Fig. 3).

Figure 6 to Fig. 8 show a combination of 2^{nd} mode of IL response and 3^{rd} mode of CF response. Fig. 9 to Fig. 11 show a combination of 1^{st} mode of IL response and 2^{nd} mode of CF response. It is expected that test 1005, 1010 and 1011 have the 2^{nd} mode of IL response, while the remaining tests have the 1^{st} mode of IL response. Since it is on purpose to design the tests with imposed top motions with either the 2^{nd} eigenfrequency (1.477 Hz) or the 1^{st} eigenfrequency (0.646 Hz), see Tab. 3. Further discussions will also prove this. It is discovered that the accelerometer in IL direction does not work properly for Test 1015, Test 1020 and Test 1025, it can be seen from Fig. 9 to Fig. 11. The exact reason was unclear, probably because it was not perfectly water-proofed. So the measured signal from this accelerometer are not used for further analysis.

Table 5: Comparison of eigenfrequencies.

Eigenperiod (Hz)	$f_{n,1}$	$f_{n,2}$	$f_{n,3}$
Model test	0.646	1.477	2.619
Numerical simulation	0.648	1.445	2.503

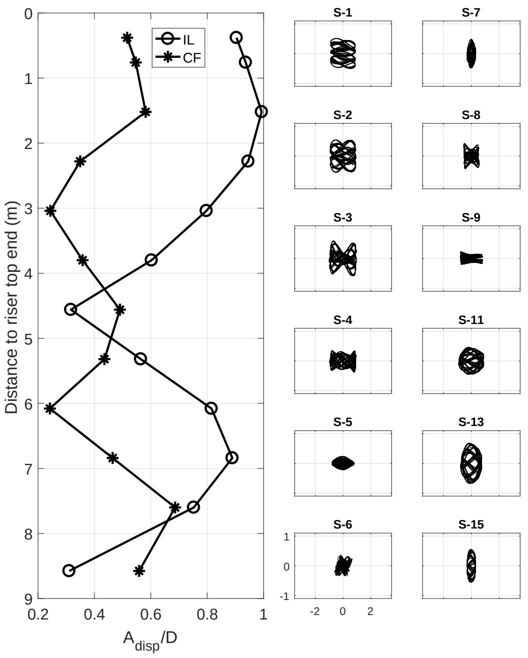

(a) Measured displacement amplitude along the riser model and orbits at locations with accelerometers.

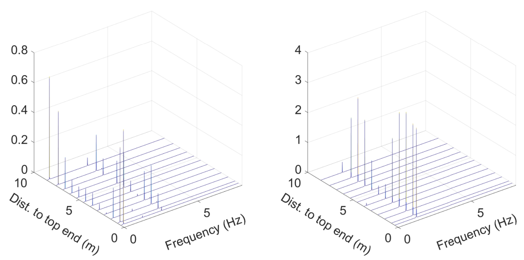

(b) PSD of displacements in CF (left) and IL (right) directions.

Figure 6: Test 1005, $A = 0.026\ m$, $T = 0.677\ s$.

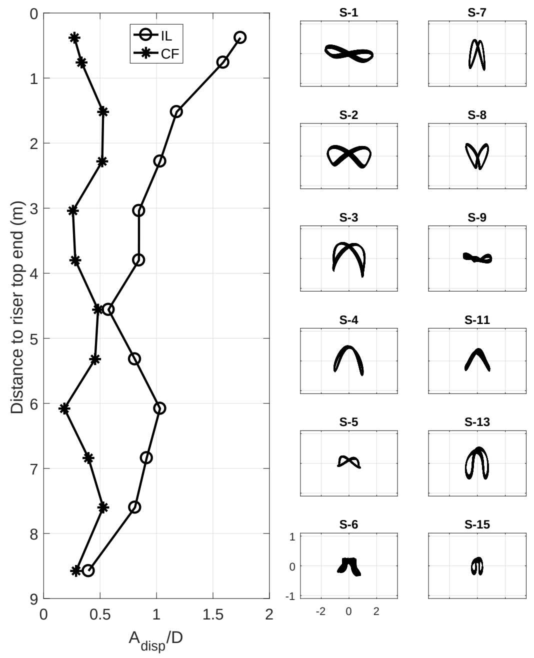

(a) Measured displacement amplitude along the riser model and orbits at locations with accelerometers.

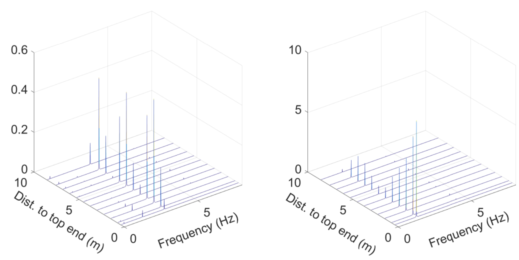

(b) PSD of displacements in CF (left) and IL (right) directions.

Figure 7: Test 1010, $A = 0.052\ m$, $T = 0.677\ s$.

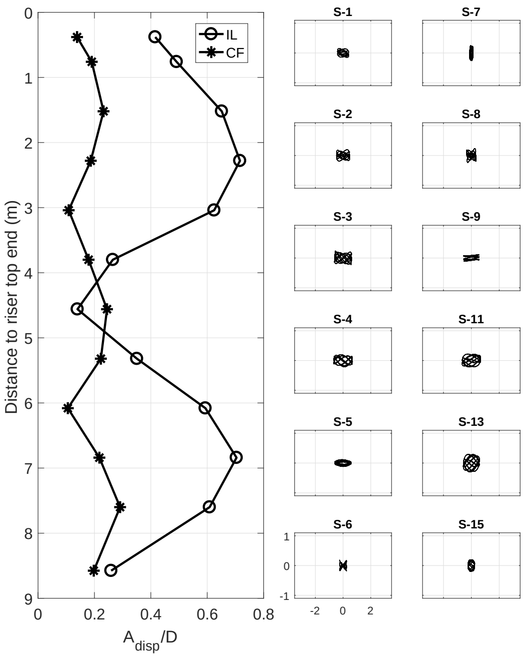

(a) Measured displacement amplitude along the riser model and orbits at locations with accelerometers.

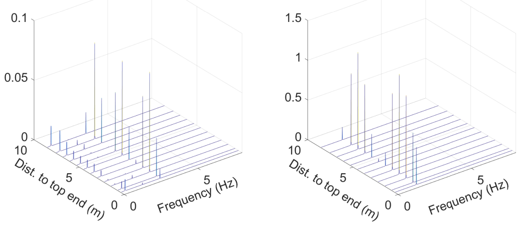

(b) PSD of displacements in CF (left) and IL (right) directions.

Figure 8: Test 1011, $A = 0.013\ m$, $T = 0.677\ s$.

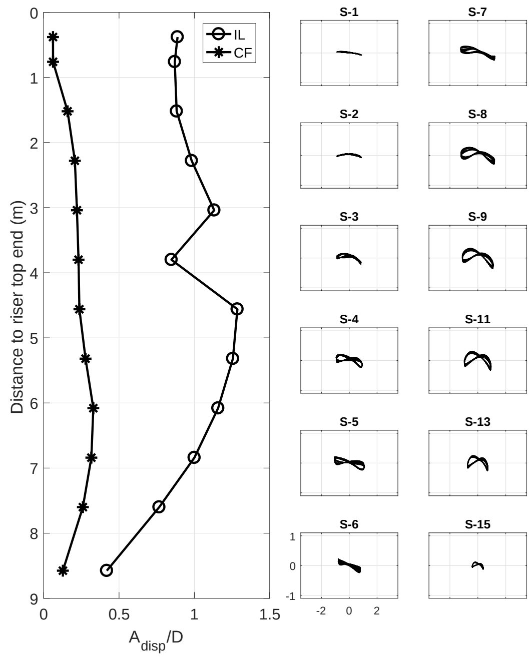

(a) Measured displacement amplitude along the riser model and orbits at locations with accelerometers.

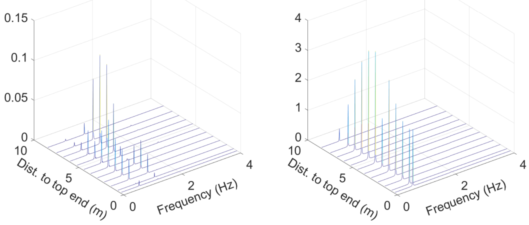

(b) PSD of displacements in CF (left) and IL (right) directions.

Figure 9: Test 1015, $A = 0.026\ m$, $T = 1.547\ s$.

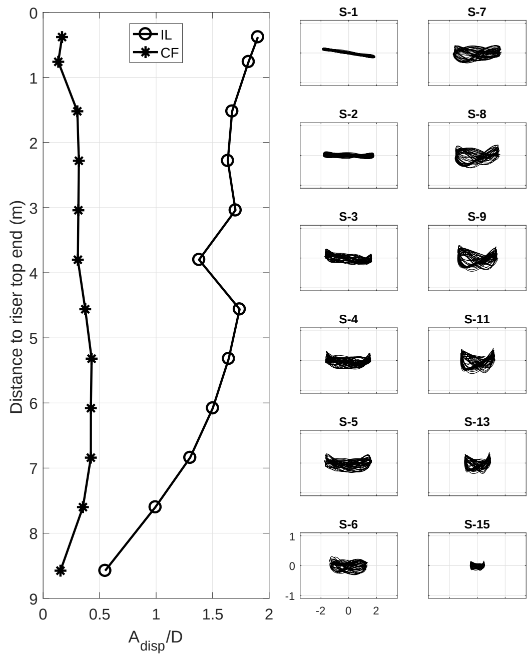

(a) Measured displacement amplitude along the riser model and orbits at locations with accelerometers.

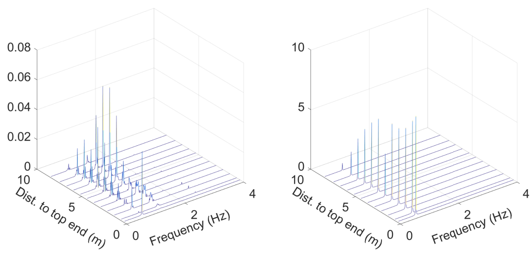

(b) PSD of displacements in CF (left) and IL (right) directions.

Figure 10: Test 1020, $A = 0.052\ m$, $T = 1.547\ s$.

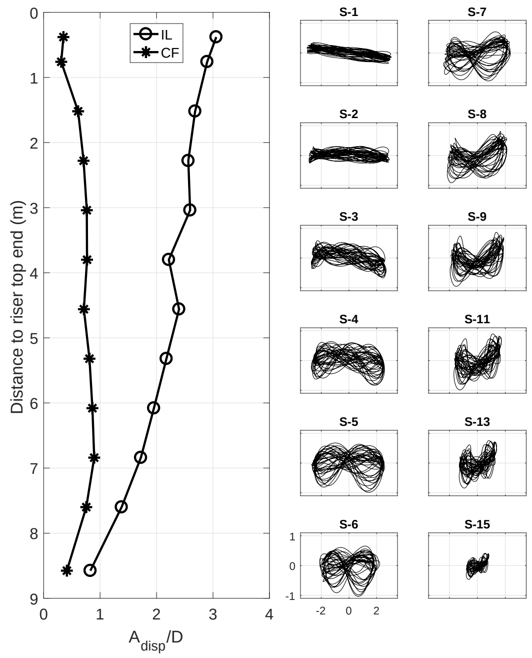

(a) Measured displacement amplitude along the riser model and orbits at locations with accelerometers.

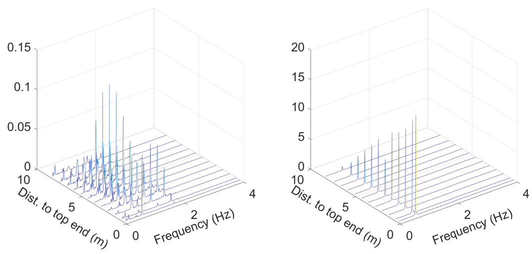

(b) PSD of displacements in CF (left) and IL (right) directions.

Figure 11: Test 1025, $A = 0.078\ m$, $T = 1.547\ s$.

5.3. IL and CF responses

Even though the forced motion is only applied in the IL direction, displacements are seen in both IL and CF directions. The riser model moves at the forced motion frequency in the IL direction. In the CF direction, the motion is approximately twice of the forced motion frequency, with several other frequencies additionally. The displacement response frequencies are summarized in Tab. 6. Results of spectral analysis on the displacement responses are shown in Fig. 6b, Fig. 7b, Fig. 8b, Fig. 9b, Fig. 10b and Fig. 11b.

The dominating CF response frequency (VIV frequency) f_{CF} is double of the IL motion frequency f_{IL} for all six cases. Multiple frequencies in CF displacement responses result in complicated cross-sectional oscillation orbits, see Fig. 6a and Fig. 8a. Single frequency displacement responses will give '8-shape' orbits, see Fig. 7a.

The relationship between CF vibration frequency and the oscillatory flow frequency was defined by Sumer and Fredsøe (1988):

$$N = \frac{f_{CF}}{f} = \frac{f_{CF} DKC}{\dot{x}_m} \tag{10}$$

where N is the number of vibrations in one cycle of oscillating flow, $\dot{x}_m$ is the amplitude of the oscillating velocity.

If we insert the corresponding values of Test 1010 into Eq. 7, we will get $N = 2$. It is noted that the response pattern for a constant KC number varies with the reduced velocity.

The six tests studied in the present paper have KC number from 5 to 18. In this KC number range, the vortex pattern are asymmetric pair of vortices in one cycle, , see Tab. 1 (Sarpkaya, 1976; Williamson, 1985), and therefore, the frequency ratio $f_{CF}/f = N = 2$.

It is important to note that the KC number decreases to zero along the drilling riser from the top end to the bottom end. When KC number is smaller than 4, the force in CF direction is minimal (Blevins, 1990). That explains the multiple frequencies in CF for Test 1005 and 1011, see Tab. 4, Fig. 6a and Fig. 8a. For Test 1010 (Fig. 7a), the maximum KC number is 11.67, vortex pairs are shed alternately into the wake during each half-cycle of oscillation, resulting distinct CF forces which has twice the frequency of IL oscillation, see Tab. 4.

The measurement signals of S-3 of Test 1010 is plotted in Fig. 12, together with the top motion history. In general, all the test cases have relatively low KC number (<20), Test 1010 has a KC number of 11.67, see Tab. 2. We can see that the CF responses are stable, without amplitude modulation. Similar responses were discovered at small KC number in Fu et al. (2014). It is probably due to that at small KC number, the vortex shedding is strengthened by its wake.

5.4. IL response amplitude comparison

IL displacement amplitude comparison is shown in Fig. 13. IL curvature amplitude comparison is

Table 6: Response frequency.

Test	V_r [-]	$f_{IL} = f$ [Hz]	f_{CF} [Hz]	$f_{CF,l}$ [Hz]
1005	13.3	1.48	2.77	0.18, 1.48
1010	26.7	1.48	2.95	1.48, 0.22
1011	6.7	1.48	2.67	0.29, 1.48
1015	5.8	0.65	1.29	0.65
1020	11.7	0.65	1.29	0.65
1025	17.5	0.65	1.28	0.65, 1.75, 0.83, 0.45, 0.18

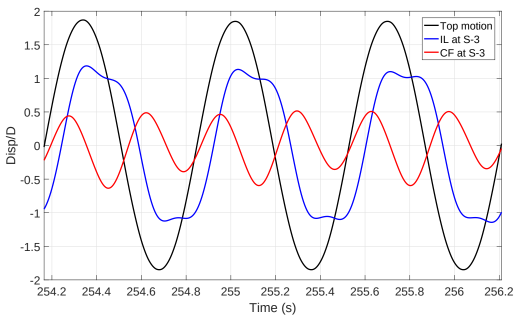

Figure 12: Time history within 3 cycles of Test 1010, at S-3.

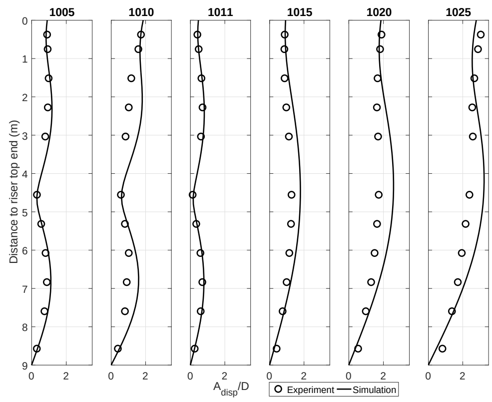

Figure 13: Comparison of IL displacement amplitude.

shown in Fig. 14. From both figures, the second mode responses are observed for Test 1005, Test 1010 and Test 1011; while the other three tests have IL responses dominated by the first mode. RIFLEX simulation over-predict both displacements and curvatures slightly, which gives conservative estimation.

The curvature amplitude comparison in Fig. 14, on the lower part of the riser (6 to 8 m from the riser top end), larger differences are observed for the first three tests. The experimental measurements indicate higher mode curvature may exist in addition to the primary mode curvature signal, however, RIFLEX seems only capture the dominating mode curvature.

5.5. *Cross flow VIV modelling*

To study the CF VIV, time domain model developed by Thorsen et al. (2014, 2016) is used. It is based on Morison's equation, with an additional term representing the lift from vortex shedding. The magnitude of the vortex shedding force is given by a dimensionless coefficient, C_v, and a value of 1.3 is adopted in this study. The drag coefficient has a value of 1.0 in this study. This model allows time varying flow around the structures, it has been validated against some experiments with oscillating flow (Thorsen et al., 2016). The synchronization model within the hydrodynamic load

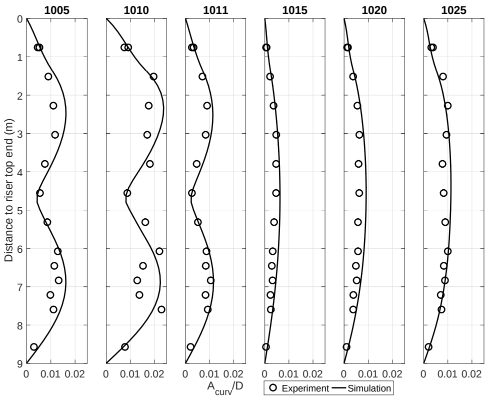

Figure 14: Comparison of IL curvature amplitude.

model is able to capture the vortex shedding process in oscillatory flow. It is important to note that the present time domain model only predict the CF VIV responses.

Selected results are presented in Fig. 15, Fig. 16 and Fig. 17.

Figure 15 shows the time history of the IL and CF responses at S-3 together with the top motion, in addition, spectral analysis is shown in the lower plot in the same figure. It is observed that dominating frequency of the CF VIV responses is double of the IL forced motion frequency, which agrees very well with the experimental measurements, see Tab. 4. In addition, strong low frequency component is also observed, which causes that the CF VIV responses have non-zero mean position. The magnitude of the vortex shedding force is proportional to the relative velocity between the oscillating riser model and the flow. A strong vortex will shed when the relative velocity is high, and a weak vortex shedding occur when the relative velocity is low. Since the CF frequency is twice the IL frequency, two vortices are shed per flow reversal. If one vortex is stronger than the other, the mean value taken over one single period will be non-zero. From Tab. 1, we know that asymmetric pair of vortices are shed during the oscillation cycle at the present KC number. And over many such cycles you could get a low frequency motion, because the timing is not exactly equal for each cycle, which means the relative strength of these vortices will vary.

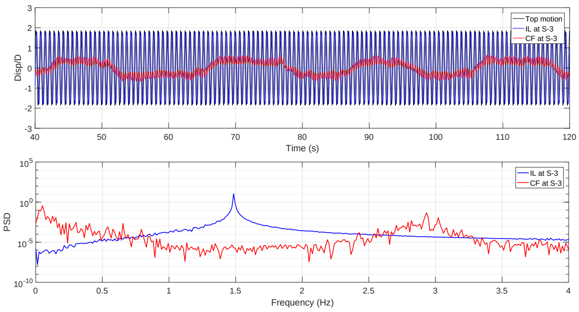

Figure 15: Time domain CF VIV simulation results: time history of top motion and IL and CF motions at S-3 (upper), spectral analysis (lower).

Time history within three cycles of two separate time windows are presented in Fig. 16 and Fig. 17. If we look at the predicted CF VIV responses, Fig. 16 has positive mean value, while Fig. 17 has negative mean value. Moreover, the phase angle between the IL and CF motions are shifted with 180 degrees. Such phase shift was not observed in the experiments. Further studies are needed to investigate whether it is physical or numerical. The predicted amplitude is around 0.6D, which is higher than model test (0.5D), see Fig. 7a.

The comparison of CF VIV amplitude ratio between model test and time domain VIV simulation is shown in Fig. 18. It shows that, using the present input coefficients in Tab. 4 in the time domain VIV

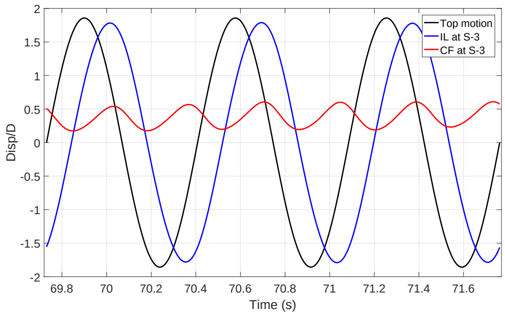

Figure 16: Time domain CF VIV simulation results within 3 cycles of Test 1010, at S-3, selected time window 1.

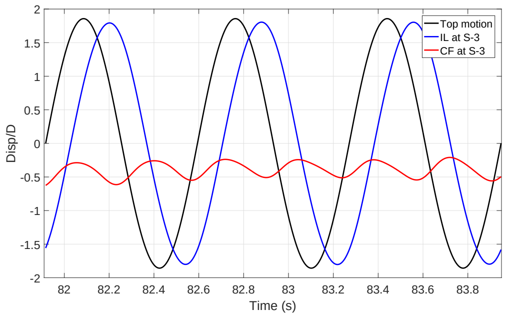

Figure 17: Time domain CF VIV simulation results within 3 cycles of Test 1010, at S-3, selected time window 2.

prediction tool, the CF VIV amplitude is overestimated, which is conservative. Another observation is that time domain VIV prediction does not capture the same mode order as the model test. It seems that time domain VIV tool predict the 2^{nd} mode in CF, while model test results show clearly the 3^{rd} mode. It is expected that the comparison can be improved by optimising the input hydrodynamic parameters, but no attempt has been done at this stage. On the other hand, the time domain VIV prediction tool is semi-empirical, relying on the experimental hydrodynamic coefficients. Enriched hydrodynamic coefficients database could also improved the prediction.

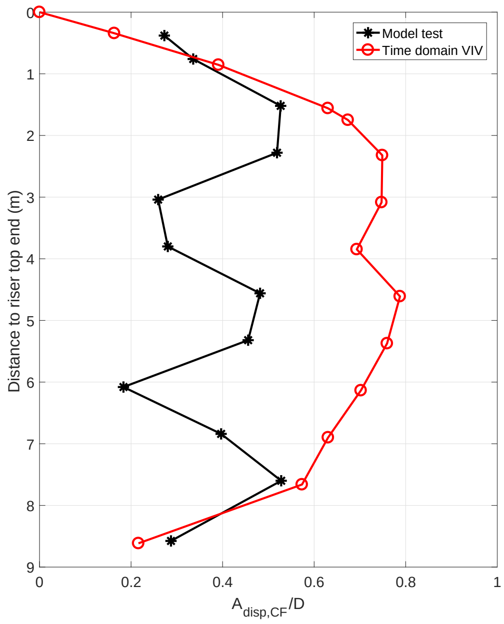

Figure 18: Comparison of CF VIV amplitude ratio along the riser. Model test vs. Time domain CF VIV, Test 1010.

6. Conclusions

A comprehensive drilling riser model test program was performed by a joint industry project funded by Statoil and BP. The model tests were carried out at MARINTEK's towing tank (now SINTEF Ocean) extension in February 2015. Six drilling riser configurations were modelled and tested. Bending strain and accelerations along the drilling riser model in both IL and CF directions were measured by strain gauges, accelerations in both directions were measured by accelerometers. Forces were measured at specific locations. The model tests have simplified but well-defined drilling riser models, covering extensive environmental conditions. The model test data forms a good database, which can be used in many ways, and these help to further understand the complicate responses of typical drilling risers.

This paper studies the TTR model. One DOF harmonic horizontal forced motions were imposed on the top end of the riser model by an actuator. The IL responses are induced by the top motion. Eigen-value analysis and non-linear time domain analysis have been carried out by using a riser system analysis program RIFLEX. Key results such as displacement and curvature amplitudes along the riser from model tests are compared with the numerical simulations. Orbits at measurement locations and spectral analysis results along the riser are presented in addition. In most of the selected cases, RIFLEX over-predicts the displacement and curvature amplitude, indicating conservative prediction.

Responses in CF direction are measured, which are caused by VIV due to oscillatory flow. The test cases have relative low KC number, the VIV responses are stable. Even the amplitude of CF VIV responses are much smaller than the IL responses, since the frequency is double as the IL frequency, the CF VIV responses may cause significant fatigue damage. A recently developed time domain VIV prediction tool is applied to simulate the CF VIV caused by the harmonic IL top motion. The result is promising, the CF VIV frequency is predicted correctly. The CF VIV displacement amplitude is over-predicted, which will give conservatism in practice.

ACKNOWLEDGEMENTS

The authors would like to thank Statoil and BP for their support and allowing the publication of the present paper, their contribution and comments on this study are highly appreciated.

References

Aronsen, K. H., 2007. An experimental investigation of in-line and combined in-line and cross-flow vortex induced vibrations. Ph.D. thesis, Norwegian University of Science and Technology, Norway.

Aronsen, K. H., Larsen, C. M., 2007. Hydrodynamic coefficients for in-line vortex induced vibrations. In: ASME 2007 26th International Conference on Ocean, Offshore and Arctic Engineering. No. OMAE2007-29531.

Blevins, R. D., 1990. Flow-Induced Vibration, 2nd Edition. Krieger Publishing Company, Kriegerdrive, Florida, USA.

Faltinsen, O. M., 1993. Sea Loads on Ships and Offshore Structures. Cambridge University Press.

Fu, S., Wang, J., Baarholm, R., Wu, J., Larsen, C. M., 2014. Features of vortex-induced vibration in oscillatory flow. ASME. J. Offshore Mech. Arct. Eng. 136, 011801.

Grytøyr, G., Hørte, T., Russo, M., Gregersen, K., Aronsen, K. H., 2017. Comparison of global riser analysis to full scale measurements on the ncs. In: ASME 2017 36th International Conference on Ocean, Offshore and Arctic Engineering. No. OMAE2017-61638.

Guo, H., Zhang, L., Li, X., Lou, M., 2013. Dynamic responses of top tensioned riser under combined excitation of internal solitary wave, surface wave and vessel motion. J. Ocean Univ. China 12 (1), 6–12.

Jung, D., Lee, H., Kim, H., Moon, D., 2012. Study of vortex-induced vibrations in a riser under low keulegan-carpenter numbers. In: Proceedings of the Twenty-second (2012) International Ocean and Polar Engineering Conference. Vol. 2. Kona, Hawaii, USA, pp. 212–219.

Kwon, Y., Kim, H., Jung, D., 2015. A study for forced oscillation experiment for OTEC riser under current. In: Proceedings of the Twenty-fifth (2015) International Ocean and Polar Engineering Conference. Vol. 2. Kona, Hawaii, USA, pp. 212–219.

Meng, S., Zhang, X., Che, C., Zhang, W., 2017. Cross-flow vortex-induced vibration of a flexible riser transporting an internal flow from subcritical to supercritical. Ocean Engineering 139, 74 – 84.

Sarpkaya, T., 1976. In-lind and Transvers Forces on Smooth and Sand-Roughened Cylinders in OscillatoryFflow at

High Reynolds Number. techreport NPS-69SL76062, Naval Postgratuate School, Monterey, California.

Shi, C., Manuel, L., 2017. An empirical procedure for fatigue damage estimation in instrumented risers. J. Offshore Mech. Arct. Eng 139, 031701–031701–8.

SINTEF Ocean, 2017a. RIFLEX 4.10.0 Theory Manual. Trondheim, Norway.

SINTEF Ocean, 2017b. SIMA 3.4 User's Guide. Trondheim, Norway.

Sumer, B. M., Fredsøe, J., 1988. Transverse vibrations of an elastically mounted cylinder exposed to an oscillating flow. ASME. J. Offshore Mech. Arct. Eng. 110, 387–394.

Thorsen, M., Sævik, S., Larsen, C., 2014. A simplified method for time domain simulation of cross-flow vortex-induced vibrations. Journal of Fluids and Structures 49, 135 – 148.

Thorsen, M., Sævik, S., Larsen, C., 2016. Time domain simulation of vortex-induced vibrations in stationary and oscillating flows. Journal of Fluids and Structures 61, 1 – 19.

Tognarelli, M. A., Taggart, S., Campbell, M., 2008. Actual viv fatigue response of full scale drilling risers: With and without suppression devices. In: ASME 2008 27th International Conference on Ocean, Offshore and Arctic Engineering. No. OMAE2008-57046.

Ulveseter, J., Thorsen, M., Sævik, S., Larsen, C., 2017. Stochastic modelling of cross-flow vortex-induced vibrations. Marine Structures 56, 260 – 280.

Wang, J., Fu, S., Larsen, C. M., Baarholm, R., Wu, J., Lie, H., 2017a. Dominant parameters for vortex-induced vibration of a steel catenary riser under vessel motion. Ocean Engineering 136, 260 – 271.

Wang, J., Fu, S., Wang, J., Li, H., Ong, M. C., 2017b. Experimental investigation on vortex-induced vibration of a free-hanging riser under vessel motion and uniform current. J. Offshore Mech. Arct. Eng 139, 041703.

Wang, J., Joseph, R. S., Ong, M. C., Jakobsen, J. B., 2017c. Numerical investigation on vessel motion-induced VIV for a free hanging riser under small Keulegan-Carpenter numbers. In: ASME 2017 36th International Conference on Ocean, Offshore and Arctic Engineering. No. OMAE2017-61705. Trondheim, Norway.

Williamson, C., 1985. Sinusoidal Flow Relative to Circular Cylinders. Journal of Fluid Mechanics 155, 141.

Yin, D., Lie, H., Russo, M., Grytøyr, G., 2018a. Drilling riser model tests for software verification. ASME. J. Offshore Mech. Arct. Eng. 140, 011701.

Yin, D., Passano, E., Larsen, C. M., 2018b. Improved in-line VIV prediction for combined in-line and cross-flow VIV responses. ASME. J. Offshore Mech. Arct. Eng. 140, 031802.

Yin, D., Passano, E., Lie, H., Grytøyr, G., Aronsen, K., Tognarellic, M., Kebadzed, E. B., 2018c. Dynamic response of a top-tensioned riser under vessel motion. In: Proceedings of the Twenty-eighth (2018) International Ocean and Polar Engineering Conference. No. 2018-TPC-0184. Sapporo, Japan.

Yuan, Y., Xue, H., Tang, W., 2017. An improved time domain coupled model of cross-flow and in-line vortex-induced vibration for flexible risers. Ocean Engineering 136, 117 – 128.